Efficiency of the vacancy pipe diffusion along an edge dislocation in MgO

Marie Landeiro dos Reis, Philippe Carrez, Patrick Cordier, Yvelin Giret

Computational Materials Science 211 (2022) 111490

Contents lists available at ScienceDirect

Computational Materials Science

journal homepage: www.elsevier.com/locate/commatsci

Full length article

Efficiency of the vacancy pipe diffusion along an edge dislocation in MgO

Marie Landeiro Dos Reis [a,b], Yvelin Giret [a], Philippe Carrez [a,*], Patrick Cordier [a,c]

[a] Univ. Lille, CNRS, INRAE, Centrale Lille, UMR 8207 - UMET - Unité Matériaux et Transformations, F-59000 Lille, France
[b] La Rochelle Université, Laboratoire des Sciences de l'Ingénieur pour l'Environnement, UMR CNRS 7356, Avenue Michel Crépeau, F-17000 La Rochelle, France
[c] Institut Universitaire de France, 1 rue Descartes 75005 Paris, France

ARTICLE INFO

Keywords:
Dislocation
Vacancies
Pipe diffusion
Kinetic Monte Carlo
Atomistic simulations

ABSTRACT

This study focuses on the mechanisms of pipe diffusion and the kinetic of point defect diffusion along dislocation line in MgO. We developed a numerical approach, based on atomic scale calculations and the use of the elasticity theory, to determine the migration energies of point defects. The kinetic of diffusion along the dislocation is then evaluated according to a on-lattice atomistic kinetic Monte Carlo algorithm informed by atomistic simulations. We show that edge dislocation in MgO behaves as a strong sink for vacancies which, combined with a lower migration energy at dislocation core region, strongly enhances the diffusion of point defect in the vicinity of the dislocation with respect to the bulk material. At low and intermediate temperatures, pipe diffusion results in an increase of the diffusivity of several order of magnitude. Accounting more precisely for the effect of pipe diffusion may therefore be a key to reconcile the experimentally measured scattering of diffusivity in MgO.

1. Introduction

Dislocations are largely recognized as potential candidates for short-circuit diffusion in crystals [1]. They affect point defect diffusion not only at long range, due to their extended elastic field, but also in their close vicinity, where the atomic arrangements strongly deviates from the bulk . Indeed, these strongly distorted regions can act as a localized channel for point-defect diffusion, leading to the nowadays called *pipe diffusion* process [2]. The enhancement of diffusion in the dislocation core can originate from either a highest concentration of point defects compared to the bulk, or an increase of the diffusion velocity resulting from the decrease of the activation energies along the dislocation line due to highly distorted atomic arrangements.

Precise measurements of such an acceleration of diffusion by dislocations remain a challenging task and different strategies have been proposed [3–5], such as for example the *in situ* measurements of the shrinkage rate of dislocation loops [6] or voids [7]. The acceleration of anion diffusion measured at low temperature in simple ionic compounds has been attributed to the presence of dislocations [8], where it has been observed in some cases a bent in the graph plotting the logarithm of the diffusion coefficient as a function of the reciprocal temperature (Arrhenius plot). More recently, in magnesium oxide (MgO), where vacancy mechanisms for diffusion predominate, a similar enhancement of the diffusion of oxygen at low temperature in high purity sample has been measured [9] and has been attributed to pipe diffusion and correlated to the dislocation densities [10].

From a general point of view, anion vacancy diffusion in MgO is commonly assumed to be intrinsic [9–13] while cation vacancy diffusion is supposed to be mostly of extrinsic origin at low temperature [10,14], thus explaining the fact that oxygen diffusion is orders of magnitude slower than magnesium diffusion at low temperature [9,12–17]. Consequently, the annealing of dislocation dipoles or loops enhanced by pipe diffusion is assumed to be limited and thus controlled by the self-diffusion of oxygen [18,19]. Some modelings have suggested that the diffusion coefficient for oxygen along a dislocation was more than four orders of magnitude greater than the lattice diffusion coefficient [18], while other studies argued that such an enhancement is resulting from a high dislocation density together with an activation energy for pipe diffusion close to the one in the bulk [19]. In this context, the binding of point defects to the dislocations will greatly affect the pipe diffusion process [20–23]. Since the effect of binding on the pipe diffusion can be counter-intuitive in oxides, it is important in MgO to assess the mechanisms of fast diffusion along the dislocation lines. For instance, in CeO_2, contrary to the common behavior observed in metals, the segregation of charged defects on dislocations has been shown to notably slow down diffusion [24].

In a previous study, we have shown that edge dislocation cores in MgO strongly attract vacancies, whatever their ionic character [25]. In the present work, we have modeled the self-diffusion problem along the same kind of edge dislocation. In order to follow the migration of

* Corresponding author.
E-mail address: philippe.carrez@univ-lille.fr (P. Carrez).

https://doi.org/10.1016/j.commatsci.2022.111490
Received 31 January 2022; Received in revised form 27 April 2022; Accepted 1 May 2022

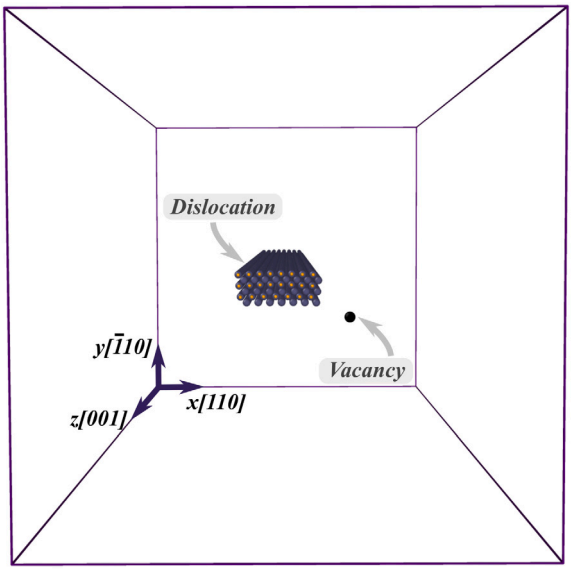

Fig. 1. View of the A-KMC simulation cell. The fully atomistically informed region (DNF: Dislocation Near Field) is here highlighted by the display of the atomic arrangement of ions, while the region informed by the anisotropic elastic theory (DFF: Dislocation Far Field) is left empty.

point defects, we rely on an on-lattice atomistic kinetic Monte Carlo algorithm (A-KMC), known to be among the simplest KMC algorithms. Yet, it has been shown to be robust and well adapted for diffusion problems [26–28]. As latter described, we have chosen to inform our KMC model with molecular static simulations and anisotropic elasticity theory to speed up our simulations. We are thus able to study long time evolutions within a system size unreachable by classical molecular dynamics investigations. We describe the used methodology in Section 2 and the results in Section 3. Finally, we discuss experimental results in Section 4 and conclude in Section 5.

2. Methodology

2.1. Kinetic monte carlo method

The geometry of our on-lattice KMC simulation corresponds to a rigid lattice of the rock-salt structure with at the center of the simulation an infinite straight edge dislocation of Burgers vector $b = 1/2[110]$, as schematically represented on Fig. 1. The orientation of the lattice is given by $x = [110]$, $y = [\bar{1}10]$ and $z = [001]$, and we consider a volume of approximately $100b * 100b * 200b$. The system is further divided into two distinct regions to account for the strong lattice distortions around the dislocation core. A central Dislocation Near Field (DNF) region is considered where the KMC lattice corresponds strictly to the atomic arrangement of the edge $1/2[110](\bar{1}10)$ dislocation. Elsewhere, in a region latter referred as Dislocation Far Field (DFF), we neglect the distortions due to the dislocation and assume a rigid lattice of perfect bulk structure. Therefore, in the DFF region, a vacancy can randomly jump to one of the atomic positions of its 12 first-neighbors, while in the DNF region the length of a vacancy hop and the number of transitions vary with the vacancy position. The size of the DNF region is chosen according to the spreading of the dislocation core and is large enough to ensure that in the DFF region the anisotropic elasticity theory can be applied to predict accurately the interaction between a point defect and the dislocation [25]. In the following, the DNF region corresponds to $12b$ along $x = [110]$, $4b$ along $y = [\bar{1}10]$ and $200b$ along $z = [001]$.

According to the transition state theory (TST), the vacancy jump frequency from a state u to a state v at a temperature T is given by:

$$\Gamma_{u\to v} = \nu_0 \exp\left(-\frac{\Delta U_m}{k_B T}\right), \tag{1}$$

where ν_0 is the attempt frequency of the hop, k_B the Boltzmann constant, and ΔU_m the corresponding internal migration energy. ν_0 being of the order of magnitude of the atomic vibrations, we further neglect its sensitivity to the temperature, and use a constant attempt frequency (≈1 THz) as commonly considered (see for instance [29]). All transitions N_{tot} from a given state u being catalogued, let $S_{\text{tot}} = \sum_{v=1}^{N_{\text{tot}}} \Gamma_{u\to v}$ be the sum of these jump frequencies. We then pick a random number $r_1 \in]0,1]$, and select the kth transition for which $S_{k-1} < r_1 S_{\text{tot}} < S_k$, where $k \in [1, N_{\text{tot}}]$ and $S_k = \sum_{v=1}^{k} \Gamma_{u\to v}$. Once selected, the corresponding transition is performed and the system is updated with a new collection of events associated with the new state. The time t is incremented by $\delta t = \ln r_2 / S_{\text{tot}}$, where $r_2 \in]0,1]$ is a second random real number [30]. To ensure statistically robust results, each set of parameters has been tested over for at least 20 independent vacancy trajectories of 10^5 KMC steps. Within the framework of TST, the migration energy ΔU_m can be expressed as the difference between the energy of the system at the saddle point of the transition and the energy of the initial state. However, as shown in the following section, ΔU_m strongly depends on the vacancy position with respect to the dislocation core position. Thus, in this study, we distinguish the case of a vacancy inside the DNF region or outside by fully computing ΔU_m atomistically in the DNF region and evaluating ΔU_m from anisotropic elastic theory in the DFF region (later quoted $\Delta \hat{U}_m$ to avoid any ambiguity).

2.2. Migration energy calculations

As mentioned above, we used two different approaches to describe hopping transitions in the DNF and the DFF regions, and performed some comparisons of these approaches in both regions. All migration energies ΔU_m in the DNF region have been determined using molecular statics simulations performed with the Large-scale Atomic/Molecular Massively Parallel Simulator (LAMMPS) package [31]. According to our previous study on dislocation/point defect interaction in MgO [25], we rely on the parameterization of a Buckingham potential for Mg and O, as proposed in [32]. Details on the basis of the simulation can be found in [25]. Vacancy hop investigations were carried out by the use of the Nudged Elastic Band (NEB) method [33,34] within a periodic simulation volume in which a dipole of edge dislocations is inserted. We carefully varied the system size to ensure that size effects on the saddle point configuration were below the force criteria of 1 meV/Å selected for the NEB calculations.

In order to drastically reduce the number of atomistic calculations for the transitions occurring in the DFF region, we rely on the elasticity theory to predict the migration barrier in the strain field of the edge dislocation. The basis of this approach is to compute the saddle point of a vacancy hop in an unstrained system, from which one can extract the elastic dipole tensor $\underline{\underline{\mathbf{P}}}^{u\to v}$ at the saddle configuration [35–37]. Knowing the energy of the initial configuration in the dislocation elastic field and its elastic dipole tensor, the migration energy writes:

$$\Delta \hat{U}_m(\epsilon_{ij}) = \Delta U_m^0 - \left(P_{ij}^{u\to v}\epsilon_{ij}(\mathbf{r}_{u\to v}) - P_{ij}^{u}\epsilon_{ij}(\mathbf{r}_u)\right), \tag{2}$$

where ΔU_m^0 is the point-defect migration energy in a unstrained bulk, $\epsilon_{ij}(\mathbf{r}_u)$ and $\epsilon_{ij}(\mathbf{r}_{u\to v})$ are respectively the strain field of the dislocation at the vacancy position $\mathbf{r}_u$ (initial state) and $\mathbf{r}_{u\to v}$ (saddle state) and finally P_{ij}^{u} and $P_{ij}^{u\to v}$ are respectively the point-defect elastic dipole tensors at the initial state (u) and at the saddle state ($u \to v$).

In this study, P_{ij}^{u} and $P_{ij}^{u\to v}$ are calculated along a NEB path describing a vacancy hop in a bulk MgO. The dislocation elastic field is assumed to be given by the anisotropic elasticity theory (see Ref. [25]). Because of the fcc symmetry of the MgO rocksalt structure, the elastic tensor at the initial state is simply given by:

$$\underline{\underline{\mathbf{P}}}^{u} = p\underline{\underline{\mathbf{I}}}, \tag{3}$$

where $\underline{\underline{\mathbf{I}}}$ is the identity matrix. At the saddle point, the elastic dipole tensor $\underline{\underline{\mathbf{P}}}$ is however anisotropic and function of the orientation of the

Table 1
Elastic dipole components of a vacancy corrected from cell size effects (See Appendix A).

Elastic dipole (eV)	V''_{Mg}	$V^{\cdot\cdot}_{O}$
p	5.35	4.88
p_1	7.53	9.31
p_2	9.79	9.38
p_3	7.48	7.23

hop. For instance in case of a vacancy jump in the [110] direction, it is of the form [35]:

$$\underline{\underline{\mathbf{P}}}^{u\to v} = \begin{pmatrix} p_1 & p_3 & 0 \\ p_3 & p_1 & 0 \\ 0 & 0 & p_2 \end{pmatrix}. \quad (4)$$

We thus computed the component p of $\underline{\underline{\mathbf{P}}}^{u}$ and the three components p_1, p_2 and p_3 of $\underline{\underline{\mathbf{P}}}^{u\to v}$ for both vacancy types (Table 1) at the initial and saddle point of a hop (See Appendix A).

3. Results

3.1. Vacancy migration energy barriers

According to the empirical potential formulation used in this study, the migration energy ΔU^0_m for magnesium vacancy and oxygen vacancy in an unstrained, bulk region of MgO are 1.53 and 1.70 eV respectively [38]. The vacancy diffusion properties being sensitive to the stress/strain field of the dislocation, the migration energies $\Delta\hat{U}_m(\epsilon_{ij})$ can increase or decrease depending on the position of the transition with respect to the dislocation. In the DFF region, we thus rely on Eq. (2) to compute $\Delta\hat{U}_m(\epsilon_{ij})$. In order to check the robustness of the elastic treatment in the DFF region, we selected different hops and compared the results with migration paths determined fully atomistically. Such a comparison is shown in Fig. 2 for a vacancy located 8 planes above the dislocation glide plane, where we can see that the evolution of the migration barriers as a function of the distance to the dislocation center is well captured by the use of anisotropic elasticity theory. As expected, far from the dislocation (*i.e.* in the outer part of our KMC simulation cell), the migration energies associated with various hops tend to become isotropic and are found to be close to the bulk energies ΔU^0_m. Closer to the dislocation, some hops can be strongly affected by the dislocation stress/strain field with an energy barrier varying by ±0.25 eV in case of transitions shown Fig. 2. Overall, Fig. 2 shows that, in the DFF region, ΔU_m is accurately given by $\Delta\hat{U}_m(\epsilon_{ij})$ as deduced from Eq. (2).

In the DNF region, partly because of the dislocation core spreading, a purely elastic treatment cannot be applied and a full atomistic description of the migration path is mandatory. It is typically the case for diffusion events occurring along the three first atomic planes below and above the dislocation glide plane (see Fig. 3). For migration events in these planes and in the DNF region, we therefore computed all the possible transitions atomistically.

As demonstrated by our previous study on the interaction between point defect and edge dislocation core in MgO [25], the first atomic planes below and above the glide plane are highly attractive for both vacancy types (V''_{Mg} and $V^{\cdot\cdot}_{O}$) with attractive sites spread up to 10 atomic rows away from the dislocation center. We show in Fig. 4 the minimum energy path computed by the climbing NEB method for three transitions for a vacancy located inside the dislocation core at the most attractive positions (position quoted 1 or 1* in Figs. 3 and 4(c)). As we can see, the transition from site 1 to site 1* is the most favorable transition. This transition tends to trap the vacancy inside the core at the most favorable sites (1 and 1*). Transitions from site 1 to site 6 or from site 6 to site 1, with migration energies around 0.5 eV, are among the most favorable events. Such events also participate to the vacancy entrapment by the dislocation core. The hop from site 2 to site

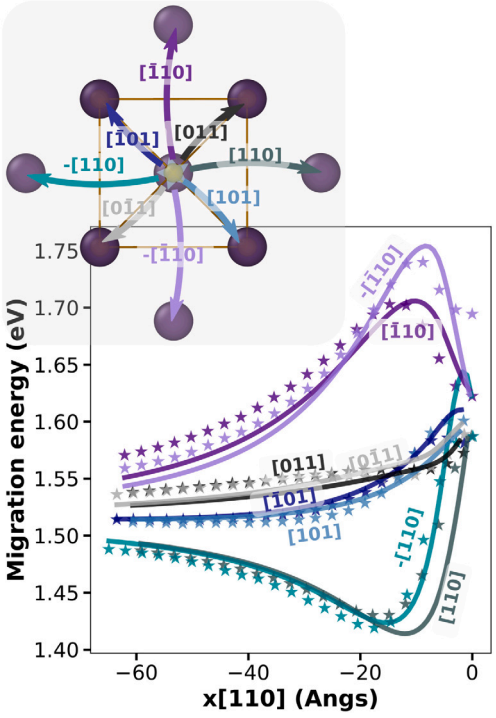

Fig. 2. V''_{Mg} migration energies along the [110] direction as a function of the distance from the projection of the dislocation center (on the right). Calculations are done for a vacancy located 8 planes above the dislocation glide plane. Because of the symmetry in the ±[001] directions, we considered 8 possible hops at each position, as represented in the upper left corner. The straight lines correspond to the results $\Delta\hat{U}_m$ obtained from elasticity theory, while symbols refer to ΔU_m computed from atomistic simulations.

1 is different from the previous events since it involves a displacement along the dislocation line: it can be considered as a pipe diffusion event. It is characterized by energy barriers of ~0.5 eV from site 2 to site 1 and of ~1.35 eV for the reverse hop. In any case, the transition energies are below ΔU^0_m.

We have represented in Fig. 5 the most favorable transitions for each site in the vicinity of the dislocation core. Some examples of energy barriers determined in the DNF region are also given in Table 2 and numerated following Fig. 3. We found similar results for V''_{Mg} and $V^{\cdot\cdot}_{O}$ although the exact values for migration energies are specific to the nature of the vacancy. Fig. 5 also allows to have a global vision of the kinetics of the system at low temperature, where the blue color corresponds to a transition that pushes the vacancy towards the dislocation, as opposed to the red color. The pipe diffusion events are represented by dashed arrows. The most favorable transitions (see also bold values in Table 2) for each atomic site inside the core tend to participate to the vacancy entrapment process (straight arrows). This highlights the high attraction of the two first atomic planes above and below the glide plane which constitute a kind of trapping raft. The most favorable pipe diffusion transitions occur within this strongly attractive region. The dislocation pipe radius for diffusion is within this trapping raft with a cross sectional area extending over a few tens of b along [110].

3.2. KMC simulations

We have implemented a KMC algorithm to simulate the vacancy diffusion processes for temperature ranging from 1000 K to 2500 K, every 250 K with each KMC trajectory accounting for 10^7 to 10^8 atomic jumps. Initially, a vacancy (either V''_{Mg} or $V^{\cdot\cdot}_{O}$) is randomly introduced on the edge of the simulation cell. The dislocation core being attractive

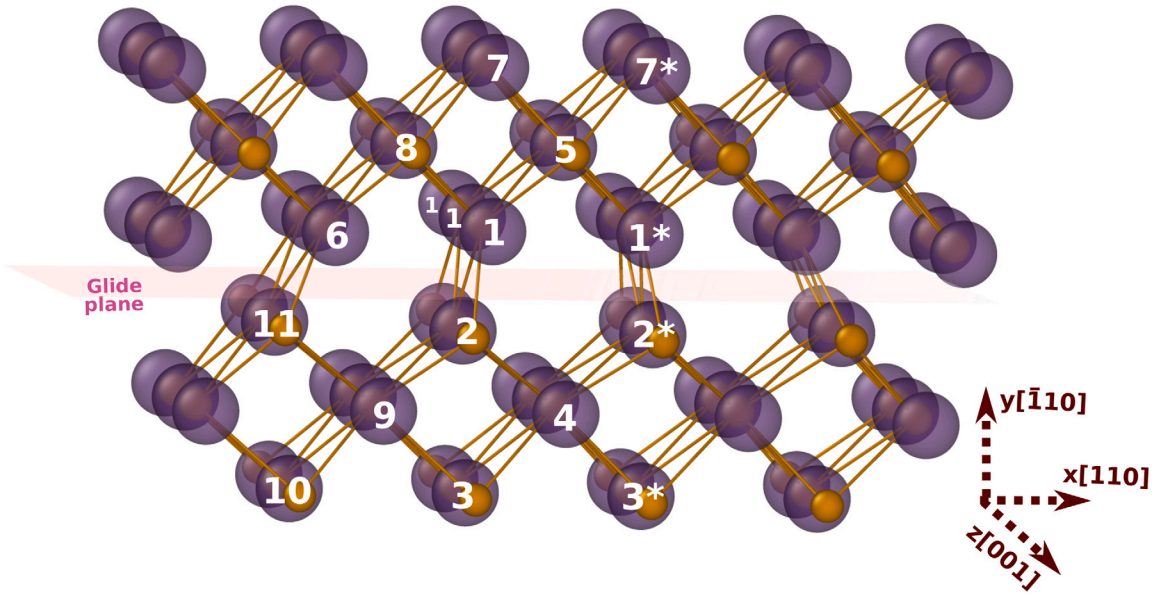

Fig. 3. Atomic sites near the dislocation core. Due to the crystal symmetry sites i are equivalent to sites $i*$. The most favorable atomic site is site 1 (thus also 1*). Initial and final hop positions are either in the same plane (constant z, hence considered as trap events), such as $1 \rightarrow 1^*$ or $1 \rightarrow 6$, or in a different plane (±[001] - pipe diffusion events), such as $1 \rightarrow 2$ or $1 \rightarrow 5$.

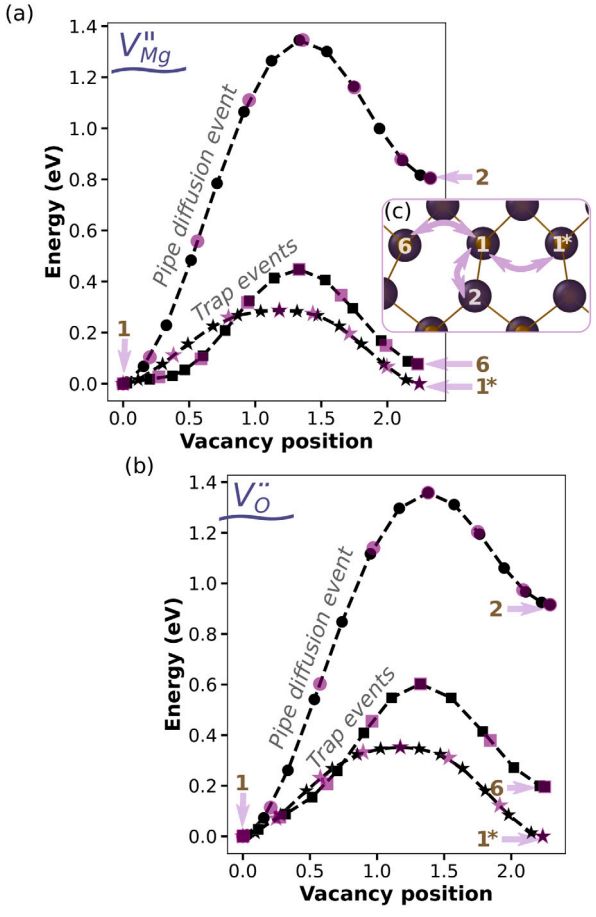

Fig. 4. Minimum energy paths (MEP) computed by NEB for the three lowest energy barriers of a vacancy initially located at the site 1 in the dislocation core (see Fig. 3). (a) corresponds to V''_{Mg} and (b) to $V^{\cdot\cdot}_O$. The corresponding jumps are represented in the subplot (c). For each of those jumps we have performed two NEB calculations: one with eight replicas (purple dots) and another with fifteen replicas (black dots). Pipe diffusion events involve a displacement component along the dislocation line while trap events do not.

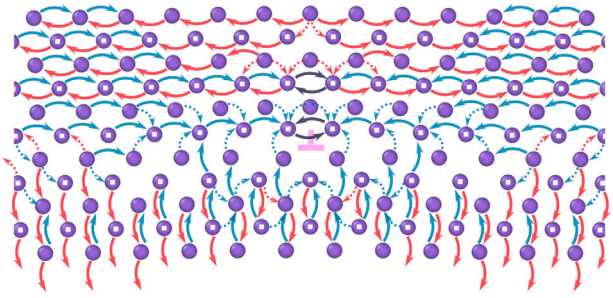

Fig. 5. Schematic representation of the most favorable transitions determined by atomistic simulations. Dashed arrows correspond to a transition that participate to pipe diffusion (±[001]), as opposed to plain arrows. The blue color corresponds to a transition that pushes the vacancy towards the dislocation, as opposed to the red color.

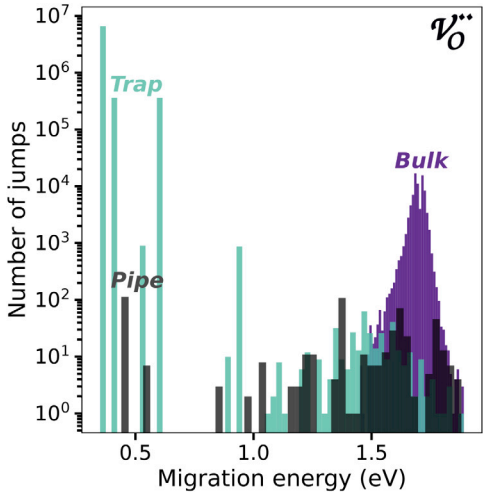

Fig. 6. Histogram of the $V^{\cdot\cdot}_O$ transition energies occurring in the vicinity of the dislocation core, as given by a KMC simulation performed at T = 1000 K. The color bars refer to diffusion events occurring either in the DFF (Bulk) region or in the DNF region. In case of events in the DNF, we distinguish the case of pipe or trap events. Details of DNF events is also given in Fig. 7.

Table 2
Some examples of vacancy migration energies near the dislocation core computed with the climbing NEB method in molecular static simulations. The atomic sites i and j selected for the transition $i \rightarrow j$ are shown Fig. 3. The most favorable transitions (<0.9 eV) are highlighted in bold. Event type 0 corresponds to trap events (initial and final hop positions are in the same xy plane), while the event type ± corresponds to pipe diffusion events (implying a change ± [001]).

Vacancy hop	Migration energy (eV)		Event
$(i \rightarrow j)$	V''_{Mg}	$V^{\cdot\cdot}_{O}$	type
1 → 1*	**0.29**	**0.35**	0
1 → 2	1.35	1.36	±
1 → 2*	2.44	2.97	±
1 → 4	2.27	2.83	0
1 → 5	1.98	2.27	±
1 → 6	**0.45**	**0.60**	0
1 → 7	2.58	2.86	0
1 → 8	1.84	2.22	±
1 → 11	3.33	3.87	±
2 → 1	**0.54**	**0.44**	±
2 → 1*	1.64	2.06	±
2 → 2*	0.91	0.99	0
2 → 3	**0.62**	**0.84**	0
2 → 4	1.17	1.40	±
2 → 6	1.23	1.66	±
2 → 9	1.15	1.32	±
2 → 11	1.22	1.31	0
3 → 2	1.19	1.11	0
3 → 3*	1.47	1.64	0
3 → 4	1.23	1.26	±
3 → 9	1.42	1.55	±
3 → 10	1.70	1.86	0

for both vacancy types [25], we observe that the vacancies tend to diffuse randomly until reaching the dislocation core and being trapped. As an example, Fig. 6 shows the histogram of all the transitions selected for $V^{\cdot\cdot}_{O}$ in our KMC simulations at $T = 1000$ K. From a general point of view, the distribution of events, here plotted as a function of their energies, shows two peaks: one centered around 1.7 eV and a larger half-peak at low energy. On one hand, events around 1.7 eV are the signature of the random diffusion of the vacancy in the DFF region. On the other hand, most of the events characterized by lower migration energies take place in the DNF region with a majority of these transitions taking place in the first atomic plane above the glide plane (Fig. 7). The vacancy trapping by the dislocation is here evidenced by the number of hops in between the two more stable positions for the vacancy (sites 1 and 1*). Although the trapping of the vacancy dominates the statistics, we observe a non negligible number of transitions leading to pipe diffusion (see for instance the number of selected transitions with migration energies of 0.4 eV or around 1.3 eV).

The same remarks can be drawn if analyzing KMC simulations ran at higher temperatures. As shown in Fig. 7 for a higher temperature (*i.e.* 4000 K), the number of transitions with higher migration energies increases dramatically, and overall, once a vacancy is trapped within the dislocation core, pipe diffusion events are still selected and see their number increased by one order of magnitude.

The analysis of the most frequent transitions (Fig. 7) reveals that the pipe diffusion path (as shown in Fig. 8) always involves hop of vacancy bound to the dislocation core in between the two first atomic plane below and above the glide plane ($n_y = 1$ and -1 following the labels introduced in Fig. 7). However, the diffusion within the dislocation core can also involve atomic planes below the glide planes down to planes quoted $n_y = 3$ in Fig. 7. Indeed, atomic planes below the glide plane correspond to a strongly attractive region for vacancy interacting with the dislocation. The pipe diffusion occurs therefore in the tensile region of the dislocation core whatever the nature of the diffusing vacancy (V''_{Mg} or $V^{\cdot\cdot}_{O}$).

A major advantage of the KMC method is to allow to compute a diffusion coefficient D_{KMC}. Indeed, at each investigated temperature,

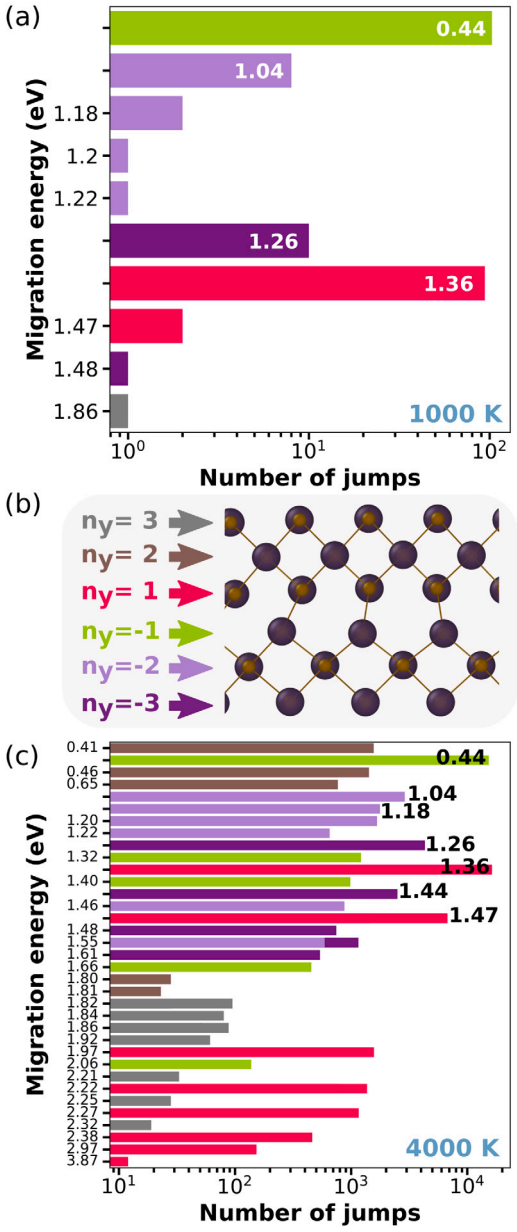

Fig. 7. Histogram of the $V^{\cdot\cdot}_{O}$ pipe transitions selected during KMC simulations performed at $T = 1000$ K (a) and at $T = 4000$ K (c). The color coding is given with respect to the initial positions of a $V^{\cdot\cdot}_{O}$ in a plane n_y before a hop as illustrated in (b).

one can define a corresponding diffusion coefficient according to the following equation [29]:

$$D_{\mathrm{KMC}} = \frac{\sum_{i=1}^{k} z_i^2(t_i)}{2t}, \tag{5}$$

where $\sum_{i=1}^{k} z_i^2(t_i)$ represents the mean square displacement (MSD) of the vacancy along the dislocation line after k steps of random walk, *i.e.* over the time t_i elapsed during a hop, t being the total time of the walk. A factor of 2 is introduced to account for the possibility of a jump along ±[001]. Fig. 9 shows an example of that calculation for both V''_{Mg} and $V^{\cdot\cdot}_{O}$. It is worth noting that the MSD plotted as a function of time shows two regimes, as revealed by the change of slope in Fig. 9. These two diffusive regimes are intrinsic to our KMC simulation setup. Indeed, the vacancy is initially introduced at the edge of the KMC simulation cell. As a consequence, we observe at the beginning of the simulation successive jumps of the vacancy in the DFF region.

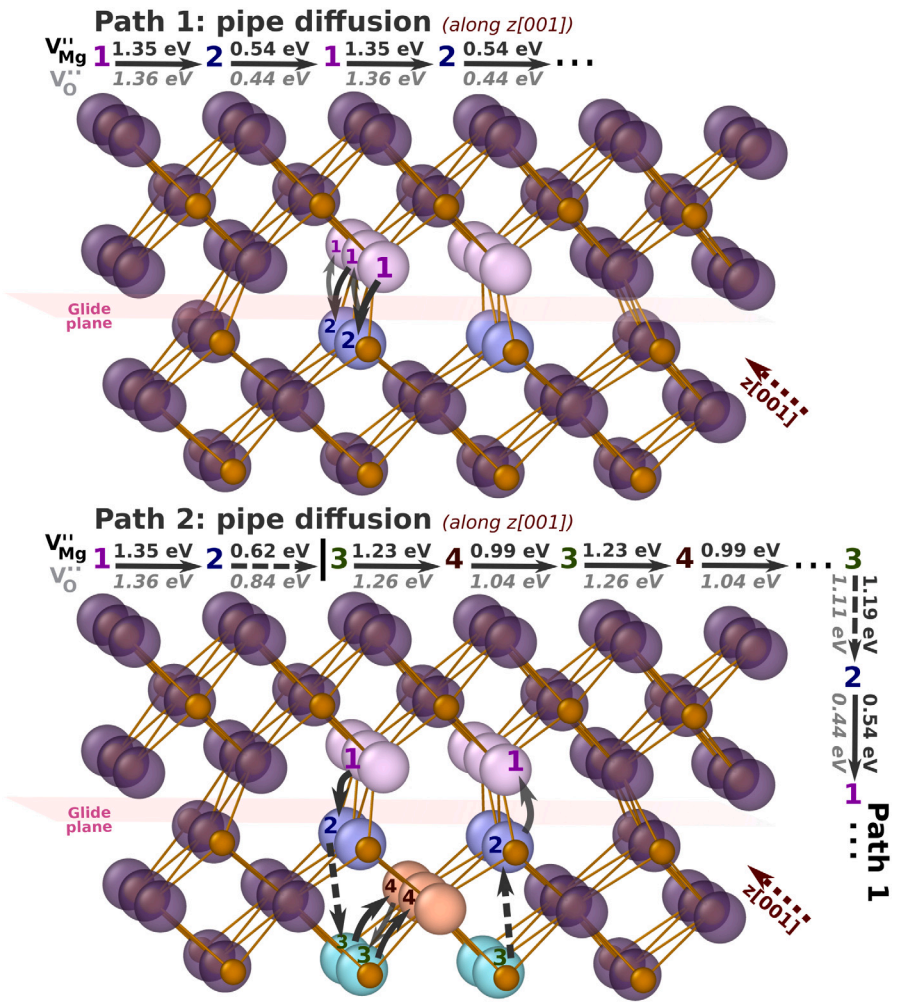

Fig. 8. Most favorable pipe diffusion paths along an edge dislocation line in MgO. The energy of each transitions are given in black and gray for V''_{Mg} and $V^{\cdot}_{O}$ respectively. Position labeled 1 is alternatively occupied by a Mg or a O atom along the [001] direction.

Despite the stress/strain field of the dislocation acting as driving force for vacancy diffusion towards the dislocation, the walk of the vacancy stays random until the trapping in the DNF region. During this first stage, D_{KMC} is close to unstrained bulk diffusivity at an equivalent temperature. By computing the MSD for several temperatures and several random seeds, we further verified that at this first stage D_{KMC} scale with $\exp\left(-\frac{\Delta U^0_m}{k_B T}\right)$, where ΔU^0_m is the vacancy migration energy as computed in a bulk system of MgO (see Table 2). As shown in Fig. 9, as soon as a vacancy (V''_{Mg} or $V^{\cdot\cdot}_{O}$) is trapped by the dislocation core (here evidenced by the sudden drop of the interaction energy), we record a strong increase of D_{KMC} corresponding to the regime of pipe diffusion. For simulations performed at low temperature, once the pipe diffusion regime is reached, it can remain until the end of the simulation. At highest temperature, the walk of vacancy being much more random, the probability of the vacancy to escape from the dislocation core increases and once it has occurred, the vacancy will walk again randomly in the vicinity of the dislocation before being recaptured at some point. As for the first stage of the KMC simulation, we can extract an apparent activation energy for the pipe diffusion regime $E^{\mathrm{pipe}}_{\mathrm{act}}$, which is averaged over the whole set of simulations performed in this study. In case of pipe diffusion of V''_{Mg}, we found an apparent activation energy of 1.38 eV. Compared to the corresponding migration energy in an unstrained bulk (1.53 eV), pipe diffusion leads to a decrease of almost 10% in activation energy for cation diffusion. The effect on anions is even more pronounced. For pipe diffusion of $V^{\cdot\cdot}_{O}$, we found an apparent activation energy of 1.33 eV comparable to the one of cations but representing here a drop of 20% of its diffusion migration energy (1.70 eV).

4. Discussion

One advantage of KMC algorithms is certainly their potentiality to span over several order of magnitude of time, thus allowing to study dynamical events unreachable through molecular dynamics. However, the accuracy of KMC is directly related to the quality of the catalog of events used as input. Here, our catalog accounts for all possible first-neighbor transitions, but relies on the quality of the empirical potential we used. Indeed, the activation energy for all transitions have been determined through the use of a Buckingham potential for Mg and O. Therefore, our choice must be questioned with at least two concerns in mind. Since we do not apply the same treatment for events occurring in the DFF and the DNF regions, the quality of our potential parameterization with respect to the migration energy of a vacancy in MgO is one concern, and a second question arises regarding its quality to describe the elastic properties of MgO crystals.

The Buckingham potential used in this study involves partial charges chosen for consistency with Bader charge analysis as determined from *ab initio* calculations [39] and has been previously applied to diffusion in MgO [32,38]. It predicts, for isolated vacancies diffusing in a unstrained MgO crystal, migration energies ΔU^0_m equal to 1.53 eV for Mg vacancies and 1.70 eV for O vacancies. A lower

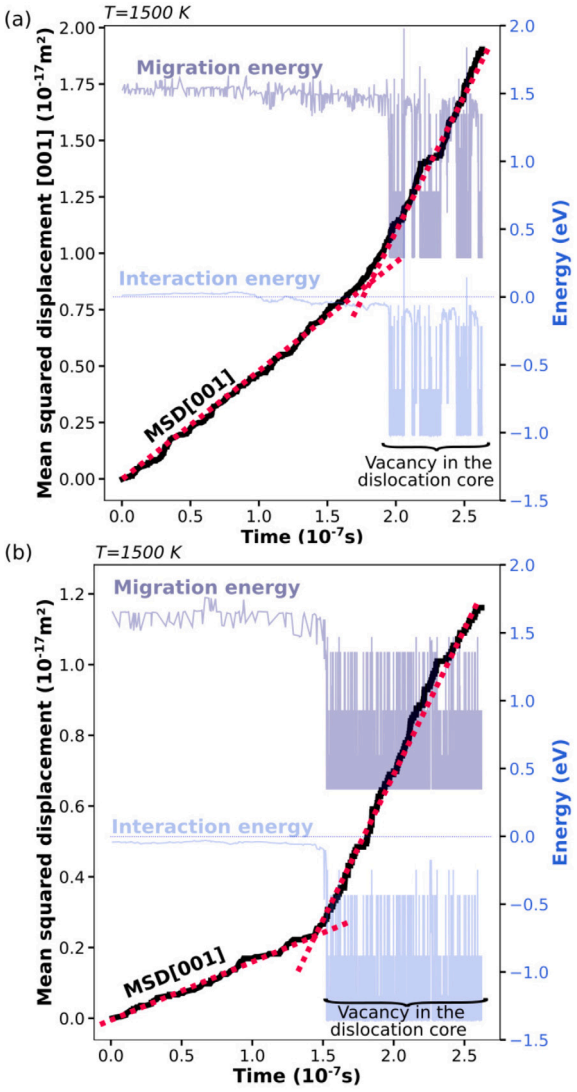

Fig. 9. Evolution of the mean squared displacement (MSD) along the dislocation line, *i.e* [001], over time at T = 1500 K. The evolution of the interaction energy dislocation/vacancy and the migration energy is also shown to demonstrate that the MSD broken slope is due to the interaction dislocation/vacancy. Case of (a) V''_{Mg} and (b) $V^{\cdot\cdot}_{O}$.

migration energy for a cation vacancy with respect to the anionic one is consistent with evidences of ionic diffusion in MgO (e.g. Ref. [9,10,12,14,15]). Nevertheless, despite the fact that the predicted ΔU^0_m remains in the range of those determined from DFT calculations, we note that our parameterization underestimates the recent DFT-GGA results. For events occurring within the core of the dislocation (*i.e.* in the DNF region), we can also note that the description of the hop from site 1 to site 2 seems to be in agreement with previous comparable investigations [40–42]. Indeed, this important hop for pipe diffusion description is characterized in our study by a migration barrier ΔU_m of 1.35–1.36 eV independently of the nature of the moving point defect. In a previous investigation of this vacancy hop inside the edge dislocation core, Rabier and co-workers [40] found comparable behaviors for V''_{Mg} and $V^{\cdot\cdot}_{O}$. In their study, the migration energy (see Table 3) was slightly higher than the one found here because of a different pair-potential parameterization. Zhang and co-workers [42], using a breathing shell model show that similar hops involve migration energies between 1.65 and 1.92 eV. Unfortunately, the path investigated in [42] corresponds to a pipe diffusion event along a dislocation core on top of its Peierls potential hill and not to a dislocation lying in its Peierls potential valley as considered here.

In the DFF region, where we compute the migration energies as given by Eq. (2), $\Delta\hat{U}_m$ relies on the evaluation of the stress–strain field of the dislocation and therefore is subjected to the accuracy of our pair potential to describe the elastic properties of MgO. As shown in Fig. 2, depending on the location of the vacancy, its migration barrier can increase or decrease with respect to the one found in an unstrained region. Therefore, any inaccuracy in the elastic compliances will be ultimately transferred to the migration energies. Based on central force considerations, our pair potential cannot reproduce the violation of the Cauchy relationship as commonly reported in MgO [43]. Yet, we assume that the order of magnitude of compliances as given by our Buckingham potential is satisfactory [43]. This assumption is supported by the fact that the elastic dipole tensors as computed here are in agreement with previous values [44]. Overall, despite the fact that the inaccuracy of $\Delta\hat{U}_m$ in the DFF region is difficult to quantify, we assume that such discrepancy only alter the dynamic of the system at the first stage of our KMC simulation until the vacancy is trapped by the dislocation core. Since we focus our study on the pipe diffusion along the dislocation, of equally importance is the fact that our pair potential is able to accurately reproduce the dislocation core structure in MgO [25,43].

The first stage of KMC simulations (see Fig. 9) corresponds to the random walk biased by the stress–strain field of the dislocation. As previously mentioned, the effect of the dislocation elastic field is to lower or to increase the migration energy depending on the position of the point defect with respect to the line. However, because the migration follows a exponential law, a decrease of the migration energy overweights any other case and as a net balance, vacancies are ultimately attracted by the dislocation. Closer to the dislocation core, such a bias can also explain the dominant pipe diffusion path (see Fig. 5) within the tensile region of the dislocation. In the mean time, the property of the dislocation core to strongly bind vacancies [25] on the two first atomic layers (below and above the glide plane) over a lengths of a few tens of b explains why, at low temperature, pipe diffusion events of type 1↔2 (Table 2) are favored. Even for long timescales accessible by our KMC simulations, this strong attraction makes events related to a diffusion along the dislocation line quite rare with respect to trapping hops. With a difference of ~1 eV in migration energy (Table 2), one may expect that diffusion along the dislocation line will never been observed by classical MD simulations. This retrospectively justifies our choice of KMC algorithm.

From mean square displacement, we find pipe diffusion activation energies $E^{\text{pipe}}_{\text{act}}$ of 1.38 and 1.33 eV for magnesium and oxygen respectively (Table 3). With respect to the bulk diffusion, the acceleration of the diffusion along a dislocation channel is thus noticeable, specially for $V^{\cdot\cdot}_{O}$. The acceleration of Mg diffusion through pipe diffusion has been experimentally quantified by Narayan [19] and latter by Sakaguchi and co-workers [4]. We find an activation energy $E^{\text{pipe}}_{\text{act}}$ for Mg in rather good agreement with the measurement of Sakaguchi and co-workers (here 1.38 eV to be compared to 1.45 eV measured experimentally). However, according to Narayan's conclusions [19], diffusion of anions can be considered as the limiting process. This is in contradiction with respect to our values of pipe diffusion activation energies which shows that activation energy for cations diffusion is slightly greater than those for anions. But, as pointed out by these authors, while it is well recognized that cation diffusion in MgO is essentially extrinsic, a strong magnesium vacancy segregation at dislocation core could explain why anions remains the limiting species. Our previous investigation of point defect segregation within the dislocation core supports this hypothesis since we measured that the interaction energy between V''_{Mg} and the dislocation can reach −1 eV [25].

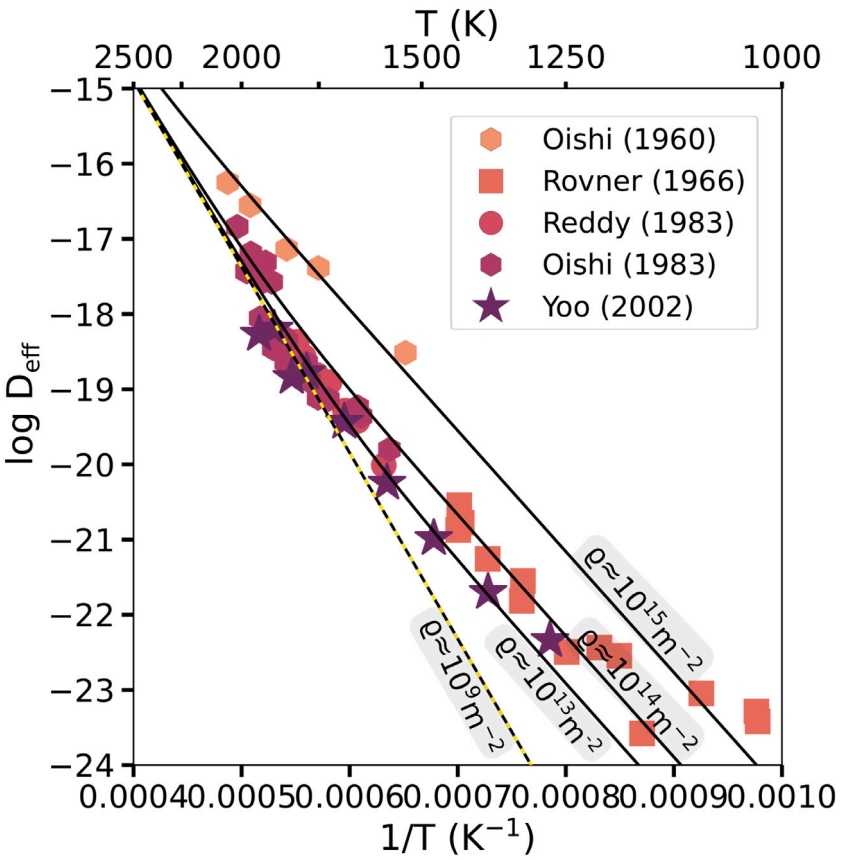

Fig. 10. Evolution of the effective diffusion coefficient D_{eff} as a function of the reciprocal temperature. D_{eff} is computed accordingly to Eq. (6) for different dislocation densities that match a summary of experimental diffusion data for oxygen in MgO. At low dislocation density (shown as a dashed line), the effect of pipe diffusion is negligible and the effective diffusion coefficient is similar to D_{bulk}.

Table 3
Comparison between the pipe diffusion migration barriers obtained in this work and determined in other theoretical studies [40,42].

Activation barriers: $E_{\text{act}}^{\text{pipe}}$ (eV)/$E_{\text{act}}^{\text{bulk}}$ (eV) – ratio (%)		
	V''_{Mg}	$V^{\cdot\cdot}_{O}$
This work	1.38/1.53 (90)	1.33/1.70 (78)
Zhang et al. [42]	1.65/1.92 (86)	1.92/2.08 (92)
Rabier et al. [40]	1.79/2.06 (87)	1.80/2.02 (89) 1.92/2.01 (96)

More generally, in MgO, one generally agrees on the intrinsic characters of O diffusion. The experimental measurements of oxygen self-diffusion coefficients show a significant scattering as reviewed in [10]. Interestingly, Van Orman proposed to reconcile the set of O diffusion coefficients by taking in account for the influence of various defects in laboratory investigated samples [10]. More precisely, he proposed to account for the effect of dislocation pipe diffusion through the evaluation of an effective diffusion coefficient D_{eff}. In order to extend the comparison of our pipe diffusion calculations to experimental measurements of oxygen self-diffusion coefficients, we can thus compute D_{eff} according to:

$$D_{\text{eff}} = D_{\text{bulk}} + \rho \cdot a \cdot D_{\text{dislo}}, \tag{6}$$

where D_{bulk} is the lattice diffusion coefficient for O in the bulk region of a MgO single crystal and D_{dislo} is the diffusion coefficient of oxygen along a dislocation core. In Eq. (6), ρ corresponds to the dislocation density within the crystal, and to account for the amount of dislocation regions, the dislocation density is multiplied by a, the cross-sectional area of a dislocation.

Both D_{bulk} and D_{dislo} are usually assumed to follow a Arrhenian dependence [10] with a pre-factor $\nu_0 b^2$ (classically of the order of magnitude of 1 cm^2/s). In case of intrinsic diffusion, one has to consider both the formation energy and the migration energy of $V^{\cdot\cdot}_{O}$. For consistency and in order to remove any adjustable parameter, we assume that the formation and migration energies are those given by the empirical potential formulation used throughout this study. Thus, we rely for D_{bulk} on a Schottky defect formation energy of 6.42 eV [38], and a migration barrier for vacancy jump of 1.7 eV. For D_{dislo}, the migration energy is taken as the pipe diffusion $E_{\text{act}}^{\text{pipe}}$ (see Table 3). Since the dislocation core region is strongly attractive for vacancy, we assume that the formation energy of $V^{\cdot\cdot}_{O}$ within the dislocation core is the one of the "bulk" reduced by the interaction energy between a vacancy and the dislocation core. Such interaction energy reaches 1.35 eV for vacancy bound to the core in site 1 or 1* (see Fig. 3) [25]. Finally, the cross-sectional area is simply considered as $a \approx \pi b^2$.

Fig. 10 shows how evolves D_{eff} in a temperature range of 1000–2500 K for three different dislocation densities, along with the experimental data for MgO single crystals. We can clearly distinguish the two contributions D_{bulk} and D_{dislo} from a bending of the effective diffusion occurring at around 1500c. At high temperature, the effect of the pipe diffusion is negligible and the diffusion mostly evolves as D_{bulk}. However, below 1500 K, the diffusion of oxygen is clearly enhanced by the presence of dislocations. As a result, the diffusion is several orders of magnitude more efficient than the one expected from a pure bulk of MgO. A rather low dislocation density (here 10^{13} m^{-2}) is sufficient to strongly modify the net effective diffusion. A larger dislocation density (*e.g.* 10^{15} m^{-2}) affects the diffusion even at temperature higher than 2000 K. We notice also the rather good agreement between

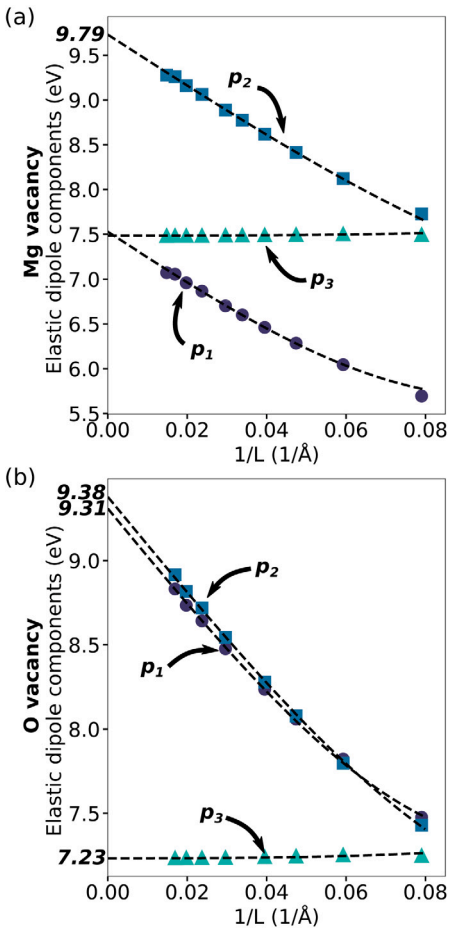

Fig. A.11. Components $p_1(L)$, $p_2(L)$ and $p_3(L)$ of $\underline{\mathbf{P}}$ at saddle point configuration plotted as a function of the cell size L. (a) and (b) correspond to the elastic dipole components of V''_{Mg} and $V^{\cdot\cdot}_{O}$respectively.

our calculations and the experimental values of oxygen diffusion. In particular, our model is able to capture the evolution of the diffusion of oxygen reported by Oishi and co-workers [12], the ones of Ready and Cooper [13] or the recent data of Yoo and co-workers [45]. Also, the scatter in oxygen diffusion coefficients can be explained at least with a reasonable amount of dislocations in the various samples used for determination. For example, by increasing the dislocation density up 10^{15} m^{-2}, our calculation of D_{eff} agrees with earlier values reported by Oishi and co-workers [46]. It should be emphasized that such an agreement with experimental data remains remarkable since our model does not include any adjustable quantities and relies on a classical pair potential formulation. Finally, one may notice that we cannot capture the lower diffusivity measured by Yang and Flynn [9]. This can be attributed mostly to our choice to rely on formation and migration energies as given by an empirical potential. For instance, we previously pointed out that the migration energy ΔU^0_m for $V^{\cdot\cdot}_{O}$ used in this work is lower than the one computed from first principles (e.g. [47] or [48]), so as the Schottky formation energy. By combining energies from various and more accurate simulations, one would expect a better agreement at low diffusivity. However, this would necessarily introduce biases and adjustable parameters.

5. Conclusion

In this study, we modeled the mechanism of vacancy pipe diffusion in MgO. Based on KMC simulations informed by atomistic calculations, we show that the dislocation acts as a strong fast diffusivity channel in MgO. The edge dislocation core behaves rather similarly for the two type of vacancies investigated here, V''_{Mg} or $V^{\cdot\cdot}_{O}$. Preferential pipe diffusion paths occur at the core of the dislocation and involve transitions through the dislocation glide plane. The activation energies of pipe diffusion as determined in this study are between 1.3 and 1.4 eV, close to the migration energies of the most frequent pipe diffusion individual event. Compared to the migration energies required in a unstrained MgO lattice, these energies are noticeably lower. At low or intermediate temperature, pipe diffusion enhances therefore the diffusivity by several orders of magnitude. We further conclude that the effect of pipe diffusion cannot be ruled out when dealing with the experimental determination of self-diffusion coefficient in MgO. The effect of pipe diffusion can be evidenced by a bending at high reciprocal temperatures of the self-diffusion coefficient. Moreover, accounting for the presence of dislocation in any investigated MgO samples, allows to rationalize the scattering in the experimental determination of oxygen self-diffusion coefficients.

CRediT authorship contribution statement

Marie Landeiro Dos Reis: Conceptualization, Investigation, Writing – original draft, Writing – review & editing. **Yvelin Giret:** Conceptualization, Investigation, Writing – original draft, Writing – review & editing. **Philippe Carrez:** Funding acquisition, Conceptualization, Investigation, Writing – original draft, Writing – review & editing. **Patrick Cordier:** Funding acquisition, Conceptualization, Investigation, Writing – original draft, Writing – review & editing.

Declaration of competing interest

The authors declare that they have no known competing financial interests or personal relationships that could have appeared to influence the work reported in this paper.

Acknowledgments

This project has received funding from the European Research Council (ERC) under the European Union's Horizon 2020 research and innovation program under Grant No 787198 TimeMan. PhC thanks the support of the French government through the Programme Investissement d'Avenir (I-SITE ULNE/ANR-16-IDEX-0004 ULNE) managed by the Agence Nationale de la Recherche, for the project named LASCO. Computational resources have been provided by the DSI-calcul intensif at Université de Lille.

Appendix A. Elastic dipole tensor calculations

The elastic dipole components are related to the stress tensor induced by the defect according to:

$$\sigma_{ij} = -P_{ij} V, \tag{A.1}$$

where V is the volume of the simulation cell. We thus computed the three components p_1, p_2 and p_3 (Table 1) for both vacancy types for an atomic configuration corresponding to the saddle point of a hop. However, since the elastic dipole tensor scales with the strain derivative of the energy, as the energy of the system containing a charged vacancy does, the elastic dipole tensor components has to be corrected from system size effects. For a non neutral periodic system, the sensitivity of $\underline{\mathbf{P}}$ to the system size results from two major contributions, (1) the elastic interaction between the defect and its periodic images [49], (2) a Coulombic interaction between the vacancy and the uniform background charge introduced to ensure a proper convergence of the electrostatic summation [50].

Fig. A.11 shows the evolution of the components $p_1(L)$, $p_2(L)$ and $p_3(L)$ as a function of the cell size L. Finite size corrections scaling with L, we applied the corrections given in [25] to correct the components of $\underline{\underline{\mathbf{P}}}$ given in Table 1.

References

[1] F. Nabarro, Steady-state diffusional creep, Phil. Mag. 16 (140) (1967) 231–237, http://dx.doi.org/10.1080/14786436708229736.

[2] J. Hirth, J. Lothe, Theory of Dislocations, Krieger Publishing Company, 1992.

[3] G. Groves, A. Kelly, Climb of dislocations in magnesium oxide, J. Appl. Phys. 33 (1) (1962) 456–460, http://dx.doi.org/10.1063/1.1777141.

[4] I. Sakaguchi, H. Yurimoto, S. Sueno, Self-diffusion along dislocations in single-crystals mgo, Solid State Commun. 84 (9) (1992) 889–893, http://dx.doi.org/10.1016/0038-1098(92)90453-G.

[5] M. Legros, G. Dehm, E. Arzt, T. Balk, Observation of giant diffusivity along dislocation cores, Science 319 (5870) (2008) 1646–1649, http://dx.doi.org/10.1126/science.1151771.

[6] J. Narayan, J. Washburn, Self-climb of dislocation loops in magnesium oxide, Phil. Mag. 26 (5) (1972) 1179–1190, http://dx.doi.org/10.1080/14786437208227372.

[7] T. Volin, R. Balluffi, Direct observation of rapid self-diffusion along dislocations in aluminum, Appl. Phys. Lett. 11 (8) (1967) 259–261, http://dx.doi.org/10.1063/1.1755125.

[8] L. Barr, I. Hoodless, J. Morrison, R. Rudham, Effects of gross imperfections on chloride ion diffusion in crystals of sodium chloride and potassium chloride, Trans. Faraday Soc. 56 (1960) 697–708, http://dx.doi.org/10.1039/TF9605600697.

[9] M. Yang, C. Flynn, Intrinsic diffusion properties of an oxide: MgO, Phys. Rev. Lett. 73 (13) (1994) 1809, http://dx.doi.org/10.1103/PhysRevLett.73.1809.

[10] J. Van Orman, K. Crispin, Diffusion in oxides, Rev. Mineral. Geochem. 72 (1) (2010) 757–825, http://dx.doi.org/10.2138/rmg.2010.72.17.

[11] L. Rovner, Diffusion of oxygen in magnesium oxide, 1966.

[12] Y. Oishi, K. Ando, H. Kurokawa, Y. Hirsco, Oxygen self-diffusion in MgO single crystals, J. Am. Ceram. Soc. 66 (4) (1983) C–60, http://dx.doi.org/10.1111/j.1151-2916.1983.tb15695.x.

[13] K. Reddy, A. Cooper, Oxygen diffusion in MgO and α-Fe_2O_3, J. Am. Ceram. Soc. 66 (9) (1983) 664–666, http://dx.doi.org/10.1111/j.1151-2916.1983.tb10618.x.

[14] B. Harding, D. Price, A. Mortlock, Cation self-diffusion in single crystal MgO, Phil. Mag. 23 (182) (1971) 399–408, http://dx.doi.org/10.1080/14786437108216393.

[15] B. Wuensch, W. Steele, T. Vasilos, Cation self-diffusion in single-crystal MgO, J. Chem. Phys. 58 (12) (1973) 5258–5266, http://dx.doi.org/10.1063/1.1679138.

[16] R. Lindner, G. Parfitt, Diffusion of radioactive magnesium in magnesium oxide crystals, J. Chem. Phys. 26 (1) (1957) 182–185, http://dx.doi.org/10.1063/1.1743247.

[17] B. Harding, D. Price, Cation self-diffusion in MgO up to 2350 °C, Phil. Mag. 26 (1) (1972) 253–260, http://dx.doi.org/10.1080/14786437208221033.

[18] H. Yurimoto, H. Nagasawa, The analysis of dislocation pipe radius for diffusion, Mineral. J. 14 (5) (1989) 171–178, http://dx.doi.org/10.2465/minerj.14.171.

[19] J. Narayan, The Kinetics of Self Diffusion and Dislocation Glide in Magnesium Oxide, Tech. rep., Lawrence Berkeley National Laboratory, 1971, LBNL Report : LBL-406. Retrieved from https://escholarship.org/uc/item/3r25v43n.

[20] C. Woo, M. Puls, M. Norgett, Energies of formation of point defects in perfect and dislocated ionic crystals, J. Phys. Colloques 37 (C7) (1976) C7–557, http://dx.doi.org/10.1051/jphyscol:19767130.

[21] M. Puls, Vacancy-dislocation interaction energies in MgO, Phil. Mag. A 41 (3) (1980) 353–368, http://dx.doi.org/10.1080/01418618008239317.

[22] M. Puls, Vacancy-dislocation interaction energies in MgO a re-analysis, Phil. Mag. A 47 (4) (1983) 497–513, http://dx.doi.org/10.1080/01418618308245242.

[23] R. Skelton, A. Walker, Interactions between bare and protonated Mg vacancies and dislocation cores in MgO, Phys. Chem. Mineral. 46 (5) (2019) 471–485, http://dx.doi.org/10.1007/s00269-018-01017-7.

[24] L. Sun, D. Marrocchelli, B. Yildiz, Edge dislocation slows down oxide ion diffusion in doped CeO_2 by segregation of charged defects, Nature Commun. 6 (1) (2015) 1–10, http://dx.doi.org/10.1038/ncomms7294.

[25] M. Landeiro Dos Reis, P. Carrez, P. Cordier, Interaction between dislocation and vacancies in magnesium oxide: Insights from atomistic simulations and elasticity theory, Phys. Rev. Mater. 5 (6) (2021) 063602, http://dx.doi.org/10.1103/PhysRevMaterials.5.063602.

[26] D. Mason, A. Sand, S. Dudarev, Atomistic-object kinetic Monte Carlo simulations of irradiation damage in tungsten, Model. Simul. Mater. Sci. Eng. 27 (5) (2019) 055003, http://dx.doi.org/10.1088/1361-651x/ab1a1e.

[27] C. Domain, C. Becquart, Object Kinetic Monte Carlo (OKMC): A Coarse-Grained Approach to Radiation Damage, Springer International Publishing, 2020, pp. 1287–1312, http://dx.doi.org/10.1007/978-3-319-44677-6_101.

[28] E. Martínez, M. Caturla, J. Marian, DFT-Parameterized Object Kinetic Monte Carlo Simulations of Radiation Damage, Springer International Publishing, Cham, 2020, pp. 2457–2488, http://dx.doi.org/10.1007/978-3-319-44680-6_137.

[29] L. Wirth, A. Farajian, C. Woodward, Density functional study of self-diffusion along an isolated screw dislocation in fcc Ni, Phys. Rev. Mater. 3 (3) (2019) 033605, http://dx.doi.org/10.1103/PhysRevMaterials.3.033605.

[30] A. Bortz, M. Kalos, J. Lebowitz, A new algorithm for Monte Carlo simulation of ising spin systems, J. Comput. Phys. 17 (1) (1975) 10–18, http://dx.doi.org/10.1016/0021-9991(75)90060-1.

[31] S. Plimpton, Fast parallel algorithms for short-range molecular dynamics, J. Comput. Phys. 117 (1) (1995) 1–19, http://dx.doi.org/10.1006/jcph.1995.1039.

[32] G. Henkelman, B. Uberuaga, D. Harris, J. Harding, N. Allan, MgO addimer diffusion on MgO (100): A comparison of ab initio and empirical models, Phys. Rev. B 72 (11) (2005) 115437, http://dx.doi.org/10.1103/PhysRevB.72.115437.

[33] G. Henkelman, B. Uberuaga, H. Jónsson, A climbing image nudged elastic band method for finding saddle points and minimum energy paths, J. Chem. Phys. 113 (22) (2000) 9901–9904, http://dx.doi.org/10.1063/1.1329672.

[34] G. Henkelman, H. Jónsson, Improved tangent estimate in the nudged elastic band method for finding minimum energy paths and saddle points, J. Chem. Phys. 113 (22) (2000) 9978–9985, http://dx.doi.org/10.1063/1.1323224.

[35] V. Borodin, A. Ryazanov, C. Abromeit, Void bias factors due to the anisotropy of the point defect diffusion, J. Nucl. Mater. 207 (1993) 242–254, http://dx.doi.org/10.1016/0022-3115(93)90266-2.

[36] M. Gillan, The elastic dipole tensor for point defects in ionic crystals, J. Phys. C: Solid State Phys. 17 (9) (1984) 1473, http://dx.doi.org/10.1088/0022-3719/17/9/006.

[37] E. Kröner, Continuum theory of defects, in: J.P. Poirier, R. Balian, M. Kléman (Eds.), Physics of Defects, Vol. 35, North-Holland, Amsterdam, 1981.

[38] S. Mahmoud, P. Carrez, M. Landeiro Dos Reis, N. Mousseau, P. Cordier, Diffusion mechanism of bound schottky defect in magnesium oxide, Phys. Rev. Mater. 5 (2021) 033609, http://dx.doi.org/10.1103/PhysRevMaterials.5.033609, URL https://link.aps.org/doi/10.1103/PhysRevMaterials.5.033609.

[39] B. Uberuaga, R. Smith, A. Cleave, G. Henkelman, R. Grimes, A. Voter, K. Sickafus, Dynamical simulations of radiation damage and defect mobility in MgO, Phys. Rev. B 71 (2005) 104102, http://dx.doi.org/10.1103/PhysRevB.71.104102, URL https://link.aps.org/doi/10.1103/PhysRevB.71.104102.

[40] J. Rabier, M. Puls, Atomistic model calculations of pipe-diffusion mechanisms in MgO, Phil. Mag. A 52 (4) (1985) 461–473, http://dx.doi.org/10.1080/01418618508237640.

[41] J. Rabier, M. Puls, Atomistic calculations of point-defect interaction and migration energies in the core of an edge dislocation in NaCl, Phil. Mag. A 59 (3) (1989) 533–546, http://dx.doi.org/10.1080/01418618908229783.

[42] F. Zhang, A. Walker, K. Wright, J. Gale, Defects and dislocations in MgO: atomic scale models of impurity segregation and fast pipe diffusion, J. Mater. Chem. 20 (46) (2010) 10445–10451, http://dx.doi.org/10.1039/C0JM01550D.

[43] P. Carrez, J. Godet, P. Cordier, Atomistic simulations of 1/2 < 110 > screw dislocation core in magnesium oxide, Comput. Mater. Sci. 103 (2015) 250–255, http://dx.doi.org/10.1016/j.commatsci.2014.10.019.

[44] M. Puls, Dipole tensors and changes in elastic constants produced by defects in ionic crystals, Phil. Mag. A 51 (6) (1985) 893–911, http://dx.doi.org/10.1080/01418618508237596.

[45] H.-I. Yoo, B. Wuensch, W. Petuskey, Oxygen self-diffusion in single-crystal mgo: Secondary-ion mass spectrometric analysis with comparison of results from gas–solid and solid–solid exchange, Solid State Ion. 150 (3–4) (2002) 207–221, http://dx.doi.org/10.1016/S0167-2738(02)00537-4.

[46] Y. Oishi, W. Kingery, Oxygen diffusion in periclase crystals, J. Chem. Phys. 33 (3) (1960) 905–906, http://dx.doi.org/10.1063/1.1731286.

[47] O. Runevall, N. Sandberg, Self-diffusion in MgO — a density functional study, J. Phys. Condens. Matter. 23 (34) (2011) 345402, http://dx.doi.org/10.1088/0953-8984/23/34/345402.

[48] M. Ammann, J. Brodholt, D. Dobson, Simulating diffusion, Rev. Mineral. Geochem. 71 (1) (2010) 201–224, http://dx.doi.org/10.2138/rmg.2010.71.10.

[49] C. Varvenne, E. Clouet, Elastic dipoles of point defects from atomistic simulations, Phys. Rev. B 96 (22) (2017) 224103, http://dx.doi.org/10.1103/PhysRevB.96.224103.

[50] M. Leslie, N. Gillan, The energy and elastic dipole tensor of defects in ionic crystals calculated by the supercell method, J. Phys. C Solid State Phys. 18 (5) (1985) 973, http://dx.doi.org/10.1088/0022-3719/18/5/005.